AADE-20-FTCE-SPP-09

Improving Cement Wellbore Integrity with Fiber Hybridization: Based on Response Surface Methodology

Phillip D. McElroy, Hossein Emadi, Marshall C. Watson, Habib K. Menouar; Texas Tech University, Lubbock, Texas. United States

Abstract

The cement sheath is paramount for wellbore integrity which provides zonal isolation (i.e. severance of fluids including gas, water, and oil), protection against corrosive fluids, and mechanical support. Failure of the cement sheath can result in damaging environmental impacts, lost revenue from production, and hazardous rig operations.

The purpose of this study is to develop a novel fiber hybridized cement class "H" mixture, embedded with alumina nanofibers (ANF's) and sol-gel treated micro-synthetic polypropylene (PP) fibers. This study involves curing the cement samples at 170°F with 3,000 psi for 24 hours and measuring the unconfined compressive strength (UCS) and dynamic modulus of elasticity (MOE) shortly after samples are demolded.

The optimum concentrations of fibers consisted of 0.15% ANF's by weight of cement (BWOC) and 0.09% PP fibers (BWOC). Due to the lack of PP fibers to resist cracks before they appear, there was minimum contribution towards obtaining ultimate UCS. ANF's were primarily responsible for reaching UCS due to their increased strength properties on the nanoscale level. However, PP fibers and ANF's simultaneously contributed towards enhancing the MOE on the nano and microscale levels. Cement samples remained in the elastic regions as the flexibility of both fibers were simultaneously utilized.

Quadratic models were effectively derived using the response surface methodology (RSM) approach. The p-value of the models were less than 0.05, according to the analysis of variance (ANOVA) table, which indicated statistical significance. The lack of fit was not significant, and the model can be used to effectively navigate the design space according to the regression model summary. Essentially, the multi-variable and multi-objective optimization analysis was effective in predicting the UCS and MOE with only a 2% variation from the experimental values.

Introduction

In order to ensure proper wellbore cement integrity, the cement sheath must provide adequate zonal isolation. Zonal isolation provides the separation of fluids (i.e. gas, water, and oil), mechanical support, and protection against corrosive fluids. Cement sheath failure can result in gas migration towards the surface, pressurization of the annulus, hazardous rig and producing operations, and lost revenue from production. The infamous blowout of Macondo, in the Gulf of Mexico (USA), was largely attributed to cement failure based upon the BP Deepwater Horizon Accident Investigation Report (Bly 2011). The cement failure led to a rig explosion occurring on April 20, 2010 killing 11 people, injuring 17 others, and causing a major oil spill. Additionally, data collected from various regions around the world (Australia, Austria, Bahrain, Brazil, Canada, the Netherlands, Poland, the UK and the USA) show that up to 75% of wells display some form of cement sheath failure (Davies et al. 2014).

Geological formation shifting and different operational procedures induce stresses on the cement sheath throughout the life of the wellbore. Various operational procedures include pressure testing, hydraulic fracturing, fluid injection, subsequent drilling, perforating, hydrocarbon production, etc. As a result, tangential, radial, and axial stresses are induced on the cement sheath (Ramos et al. 2009; Jafariesfad et al. 2017; Li et al. 2017). Figure 1 displays the mentioned stresses where ($\tau_{r\theta f}$) represents the tangential stress, (σ_{rf}) represents the radial stress, and (σ_{vc}) represents the vertical stress.

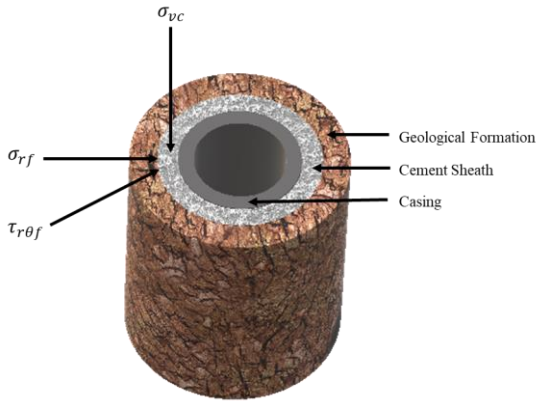

Figure 1: Tangential, radial, and axial stresses on the cement sheath

Typically, the ultimate radial stress (which is perpendicular to the axis of the wellbore) represents the compressive strength while the ultimate tangential stress (which is perpendicular from the direction of radial stress) represents the tensile strength (Mueller et al. 2004). Consequently, mechanical property (strength and elastic properties) testing of the cement sheath is conducted to assess its mechanical performance in wellbore conditions (Lavrov and Torsæter 2016).

There have been considerable research efforts devoted towards improving the cement sheaths mechanical performance using nanoparticles, nanotubes, and nanofibers (Jafariesfad et al. 2017). Compared to their counterparts, nanofibers have displayed the ability to enhance the cement sheath's mechanical performance better than nanoparticles and are less expensive than nanotubes (Khitab and Tausif 2014; Aghayan 2016). Among the various nanofibers, alumina nanofibers (ANF's) have displayed improved mechanical reinforcement due to the seeding effect, high dispersibility, and an insignificant impact on the stability performance of the cement slurry (McElroy et al. 2019; McElroy et al. 2020).

In addition to singly-reinforced cementitious additives, hybrid-reinforced cementitious additives have shown considerable potential. As an example, while using carbon nanofibers (CNFs) and polyvinyl alcohol (PVA) microfibers, ladder scale reinforcement was observed in Type I ordinary Portland cement (OPC) which significantly improved the mechanical properties of the matrix (Metaxa et al. 2010). Other researchers have conducted similar studies whereby a hybrid-reinforced cement system was found to be more effective than a singly-reinforced cement system (Yao et al. 2003; Banthia and Sappakittipakorn 2007; Hari and Mini 2019). The improvement of the hybrid-reinforced cement system as opposed to the singly-reinforced cement system is due to the gradual multi-scale failure process of cementitious material. Cement failure begins on the nanoscale level, progresses to the microscale level, and finally the macroscopic level (Metaxa et al. 2010). Fibers are able to slow the progression or halt cracks in cement due to the ability of fibers to bridge cracks and transfer loads.

Despite the amount of research conducted, there are limited studies displaying the applicability of oil well cement cured in a simulated wellbore environment (pressure and temperature conditions beyond ambient) reinforced with a fiber hybrid system. Thus, this work investigates the uniaxial compressive strength (UCS) and the dynamic modulus of elasticity (MOE) of cement class "H" reinforced with a novel fiber combination of ANF's and sol-gel treated micro-synthetic polypropylene (PP) fibers. Natural PP fibers are able to accelerate cement thickening time and increase the flexibility and chemical durability of oil well cement (Ahmed et al. 2018). However, the fiber/matrix bond of PP fibers is considerably weak (Coppola et al. 2015). Consequently, the sol-gel reaction was conducted in order to deposit nano-silica (SiO_2) on the surfaces of PP fibers which ultimately improves the bonding characteristics. Nano-silica has the ability to improve the cement slurry impermeability and increase the mechanical properties of the cement sheath (El-Gamal et al. 2017). Under the Design of Experiment (DOE) the response surface methodology (RSM) was utilized to determine the optimum dosages of fiber concentrations, considering the cement formulation is a multi-variable and multi-objective optimization design.

Experimental Methodology

Materials used

Class "H" cement, distilled water, a dispersing agent (friction reducer), and fiber additives were used to formulate cement samples. A 2% concentration of 99.9% pure gamma-aluminum oxide (γ-Al_2O_3) ANF's were pre-dispersed in deionized water. The materials used to complete the sol-gel treatment of PP fibers consisted of tetraethyl orthosilicate (TEOS, $C_8H_{20}O_4Si$, 98%), ammonium hydroxide solution (NH_4OH, 28% NH_3 in H_2O), and pure ethanol (EtOH, CH_3CH_2OH). Table 1 presents the physical properties of both fibers.

Table 1: Physical Properties of ANF's & PP fibers

Fiber	Type	OD	Length	Tensile Strength	MOE	TS	Density
ANF	γ-Al_2O_3-OH	2.7-10 nm	100-900 nm	1.74E+06 psi	5.80E+07 psi	2012°F	0.14 lb/in^3
PP	$(C_3H_6)_n$	18 µm	12 mm	8.08E+04 psi	5.95E+05 psi	334°F	0.03 lb/in^3
Note: OD-Outer Diameter; MOE- Modulus of Elasticity; TS-Thermal Stability							

Fiber functionalization

ANF's are produced by oxidizing aluminum in a controlled liquid phase and reduced to the specified size range (Table 1) by a disintegrator. Due to ANF's large aspect ratio (length-to-diameter ratio) and high Van der Waals forces, fibers readily agglomerate which can lower the mechanical properties of cement material (McElroy et al. 2019; McElroy et al. 2020). Thus, ANF's are ultrasonicated until fibers are properly dispersed and deagglomerated. In order to validate an effective ANF dispersion, transmission electron microscope (TEM) images of the pre-dispersed solution were taken. According to Figure 2, ANF's were properly dispersed.

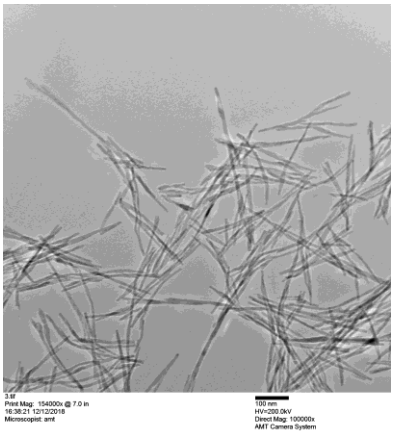

Figure 2: Pre-dispersed 2% ANF solution

Based upon previous studies (Pinto et al. 2008), SiO_2

nanoparticles were deposited on PP fibers through the sol-gel technique. Essentially, the synthesis of a colloidal suspension of solid particles (sol) in a liquid (gel) allows the hydrolysis (production of hydroxyl groups) and condensation (polycondensation of hydroxyl groups along with residual alkoxyl groups) to produce large molecules of silicon through polymerization. Figure 3 displays PP fibers prior to using the sol-gel technique.

Figure 3: As received polypropylene (PP) fibers

The sol-gel process requires immersing one gram (g) of PP fibers in 85 mL of EtOH, 9 mL of distilled water, and 1.5 mL of NH_4OH at 60°C (140°F) for 10 minutes. 4.5 mL of TEOS is then gradually added under magnetic stirring. After two hours, fibers were washed with distilled water and dried at room temperature (21.1°C (70°F)). Scanning electron microscope (SEM) images were used to validate the deposition of SiO_2 nanoparticles on the surface of PP fibers along with an energy-dispersive X-ray spectroscopy (EDX) analysis to affirm the results.

Cement samples preparation and testing procedures

Figure 4 displays the Ofite model 20 constant speed blender which was used to prepare all cement specimens.

Figure 4: Ofite model 20 constant speed blender

Distilled water was blended for 15 seconds (s) at a rotational speed of 419 rad/s. During the 15 s period, the dry blended solids were uniformly added. After the 15 seconds duration, the rotational speed is automatically increased to 1257 rad/s for 35 seconds. The produced slurry is poured into thinly greased 50.8 mm (2 inch) cubed molds (approximately 135 mL of slurry) and placed into the high temperature high pressure (HTHP) curing chamber (Figure 5).

Figure 5: High temperature high pressure (HTHP) curing chamber

Samples were cured at 76.7 °C (170 °F) with 20.68 MPa (3,000 psi) for 24 hours in order to emulate wellbore conditions. After curing, samples were demolded and the UCS was measured under a 72 kN per minute constant load rate. Figure 6 shows a result of the process. All test procedures were done in accordance with (API 10B-2 2013).

Figure 6: Result of a uniaxial compressive strength (UCS) test

In order to measure the dynamic MOE of cement samples, demolded cube specimens were sub sectioned into 38.1 mm (1.5 inch) diameter x 50.8 mm (2 inch) length cylinders using a diamond-tipped core drill bit mounted on a Wilton variable speed drill press. Cylinders were drilled using water as the lubricating fluid and dried in a vacuum oven at 100°C (212°F) over a 24-hour duration until the weight variation was less than 0.1%, a commonly used technique (Nelson and Guillot 2006). The NER Autolab 1500 (New England Research, Inc., White River Junction, VT, USA) (Figure 7) was used to

calculate the dynamic MOE.

Figure 7: NER Autolab 1500

The bulk density ($\boldsymbol{\rho}$) (g/cm^3) of the cement cores were calculated, before testing, as shown in equation (1) where "$\boldsymbol{r}$" represents the radius (cm), "$\boldsymbol{h}$" represents the height (cm), and "$\boldsymbol{m}$" represents the mass (g). Using the ultrasonic system from the NER Autolab 1500, shear pulses ($\boldsymbol{V_s}$ waves) and compressional pulses ($\boldsymbol{V_p}$ waves) were generated through cement specimens using a receiver and source transducer. Measurements were taken at a confining pressure of 20.68 MPa (3,000 psi) in which the measured velocities ($\boldsymbol{V_s}$ and $\boldsymbol{V_p}$ waves (m/s)) were used to calculate the dynamic MOE (equation (2)). All tests were conducted three times, with the average taken, to ensure repeatability.

$$\rho = \frac{m}{\pi r^2 h} \quad (1)$$

$$MOE = \frac{\rho V_S^2 (3V_P^2 - 4V_S^2)}{V_P^2 - V_S^2} \quad (2)$$

Experimental design using response surface methodology (RSM)

Since the cement mixture formulation is a multi-variable and multi-objective optimization design, the RSM through the DOE is utilized. RSM is a statistical technique in which a response of interest is optimized by analyzing several independent variables that influence the response (Montgomery 2017). Typically, the central composite design (CCD) method is used which is the most commonly utilized method for RSM problems. Essentially, a functional relationship is derived between the response and the experimental variables. A CCD is composed of k factors (independent variables) with $2k$ axial runs (star runs), 2^k factorial runs (n_F), and n_c center runs. Thus, for each CCD test 13 experimental runs were executed encompassing four axial runs, four factorial runs, and five center runs. Five center runs are recommended which effectively tests for the model's lack of fit. The factors are ANF and PP fibers with the responses as UCS and dynamic MOE. A design is made rotatable according to equation (3), in which "α" has a value of 1.414.

$$\alpha = (n_F)^{1/4} \quad (3)$$

Usually, design variables are rescaled to coded variables in a CCD with ± 1 as the factorial levels and zero as the centroid of the design. Figure 8 displays the CCD for the current scenario.

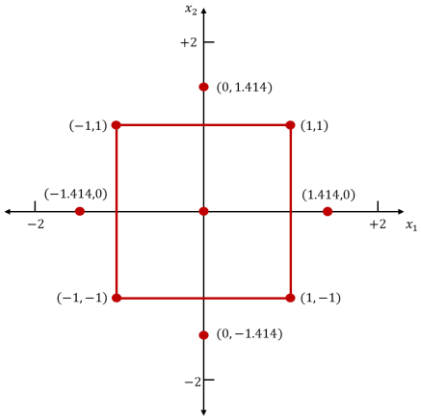

Figure 8: Central composite design (CCD) for ANF & PP fibers

Increasing the ANF dosage past 0.2% lowers the mechanical properties of the cement matrix due to nanofiber clustering and irregularities in the hydration products (Muzenski et al. 2019; McElroy et al. 2019; McElroy et al. 2020). Therefore, the maximum ANF concentration added was 0.2% and the minimum concentration added was 0.03% by weight of cement (BWOC). The minimum ANF concentration was determined based on preliminary results and was selected to remain in the optimum design region. Likewise, the maximum concentration of PP fibers added was 0.5% BWOC based on previous studies (Ede and Ige 2014; Ahmed et al. 2018). Increasing the PP fiber dosage past 0.5% BWOC results in lower cement mechanical properties and "fur balls" which tend to plug float equipment and pump plungers (Nelson and Guillot 2006). The minimum concentration of PP fibers was selected to be 0.09% BWOC, also based on preliminary tests and to remain in the optimum design region. All cement samples were designed with a water-to-cement ratio of 0.42. Table 2 displays all cement formulations according to the CCD method.

Table 2: Cement sample mixture proportions

Run Number	Factors (% BWOC)		g for 135 mL cement slurry				
	ANF's	PP fibers	Cement	Water	Dispersant	ANF's	PP fibers
1	0.03(-1)	0.09(-1)	179	76	0.71	0.05	0.16
2	0.20(1)	0.09(-1)	179	76	0.71	0.36	0.16
3	0.03(-1)	0.50(1)	179	76	0.71	0.05	0.90
4	0.20(1)	0.50(1)	179	76	0.71	0.36	0.90
5	0.00(-1.41)	0.30(0)	179	76	0.71	0.00	0.54
6	0.24(1.41)	0.30(0)	179	76	0.71	0.43	0.54
7	0.12(0)	0.00(-1.41)	179	76	0.71	0.21	0.00
8	0.12(0)	0.58(1.41)	179	76	0.71	0.21	1.04
9	0.12(0)	0.30(0)	179	76	0.71	0.21	0.54
10	0.12(0)	0.30(0)	179	76	0.71	0.21	0.54
11	0.12(0)	0.30(0)	179	76	0.71	0.21	0.54
12	0.12(0)	0.30(0)	179	76	0.71	0.21	0.54
13	0.12(0)	0.30(0)	179	76	0.71	0.21	0.54

The optimum responses are near the defined region; therefore, a second order polynomial equation was used to calculate the UCS and MOE (equation (4)).

$$y = \beta_0 + \sum_{i=1}^{k} \beta_i x_i + \sum_{i=1}^{k} \beta_{ii} x_i^2 + \sum_{j=2}^{k} \sum_{i=1}^{j=1} \beta_{ij} x_i x_j + \varepsilon \qquad (4)$$

"y" is the predicted response for each cement sample, x_i and x_j are the experimental factors, β_0 is the y-intercept of the model, β_i and β_{ii} represent the linear and quadratic coefficients respectively, β_{ij} represents the cross product coefficients, and "ε" is the residual error of the model. A software equipped with a multivariate regression package was used to fit the polynomials. The analysis of variance (ANOVA) was used to analyze the interaction between the responses and the factors.

Results and Discussion

Deposition of nano-silica (SiO_2) particles on PP fibers

Figure 9 displays the SEM and EDX results of the untreated (absence of sol-gel treatment) PP fibers.

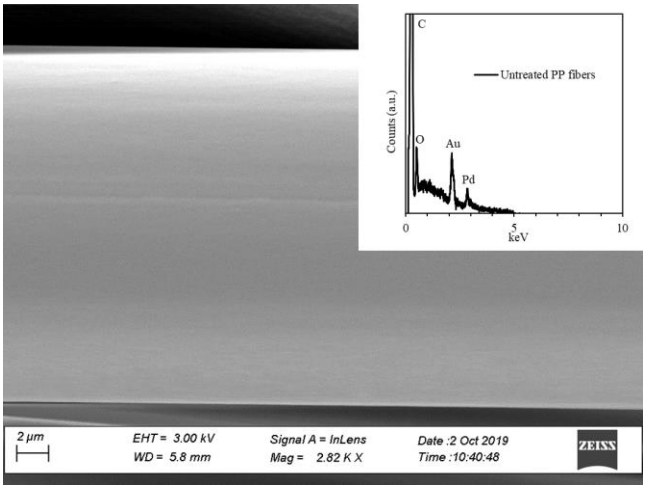

Figure 9: SEM and EDX results of untreated PP fibers

The surface of the untreated PP fibers is noticeably smooth with no apparent roughness. However, fiber roughness is beneficial for improving the cement/matrix bond which improves the cement mechanical properties. Additionally, PP fibers possess poor wettability and a differing surface energy from the cement matrix which also results in a weak fiber/matrix bond (Di Maida et al. 2015; Akhlaghi et al. 2020). Thus, the sol-gel treatment was used to effectively deposit nano-silica particles on the surfaces PP fibers in order to improve the cement/matrix bond (Figure 10).

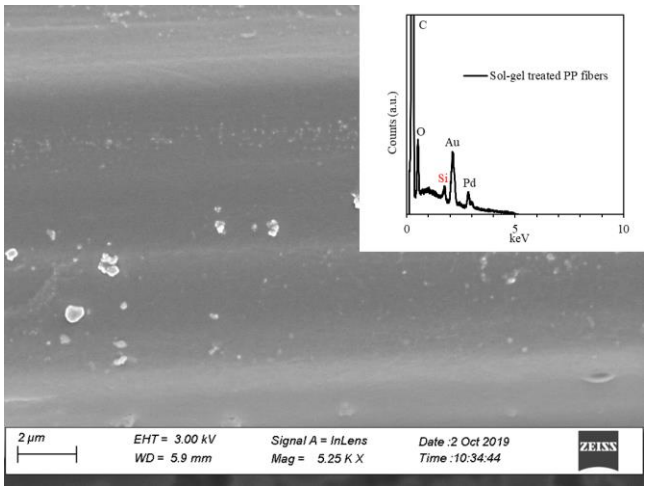

Figure 10: SEM and EDX results of sol-gel treated PP fibers

Figure 10 indicates improved roughness, due to the deposition of nano-silica particles, and the EDX results confirm the presence of silicon (Si) which was absent in Figure 9. The carbon (C) peak is due to the carbon tape (used to perform the test) and the (Au/Pd) peaks are a result of the fiber coating process before analysis. Nano-silica improves the mechanical properties, impermeability, reduces cement thickening time, and possess high pozzolanic activity. The nano-silica particles also contain silanol groups which allows points of nucleation for the formation of hydration components (Di Maida et al. 2015; El-Gamal et al. 2017). Therefore, it is widely used in the oil well cementing and construction industries. The improved characteristics are essential for maximizing the properties of oil well cement.

RSM Analysis: Uniaxial Compressive Strength (UCS)

Figure 11 displays the UCS values for the cement specimens which varied between 4033 and 5253 psi.

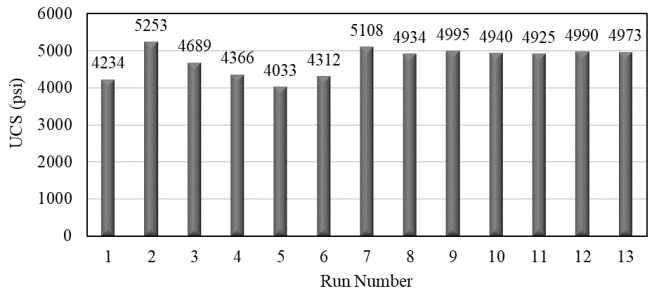

Figure 11: UCS experimental values

The values in Figure 11 were then used to develop the three-dimensional response surface plot (Figure 12).

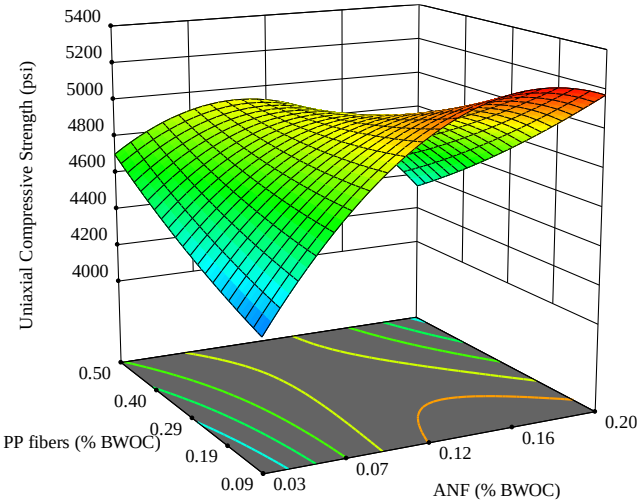

Figure 12: 3-D response surface plot, UCS

According to Figure 12, there is a slight increase in the UCS compressive strength when the concentration of PP fibers is increased. The slight strength increase is attributed to reinforcement and bridging effect of PP fibers to resist the propagation of cracks. Also, the deposition of nano-silica particles increased the adhesion between the fiber/cement matrix. This allows for a more uniform distribution of stress throughout upper and lower cement surface regions rather than at the crack tips. However, PP fibers are unable to provide significant contribution towards the UCS. This is because PP fibers provide resistance in post-cracking (after cracks have appeared) rather than before cracks appear (Pajak 2016). Also, Table 1 indicates there is a large discrepancy in the strength difference between PP fibers and ANF. The tensile strength of PP fibers is two orders of magnitude lower than ANF. Since cracks initiate at the nanoscale level, the PP fibers become ineffective at the microscale level once the reinforcement of ANF's have failed.

Instead, the results indicate, ANF's are the primary contributor for achieving ultimate UCS. ANF's provide outstanding reinforcement capabilities before cracks appear. There are several reasons for the strength enhancement: (1) ANF's possess a "bridging effect" which transfers stresses between nanopores (2) there is a nucleation effect which increases the degree of hydration (DOH) (more water is able to react with the cement) (3) the production of hydration products increases (mainly calcium-silicate-hydrate (C-S-H)) (4) the cementitious properties are increased with the formation of 1.1 nm tobermorite due to the presence of alumina (Al_2O_3) (Meller et al. 2009; McElroy et al. 2019; McElroy et al. 2020). Equation (5) is the empirically derived equation which can be used to calculate the UCS.

$$UCS\ (psi) = 3581.11626 + 20200.31727 * ANF + 1228.67952 * PP\ fibers - 19253.94548 * ANF * PP\ fibers - 55460.16919 * ANF^2 + 978.49840 * PP\ fibers^2 \quad (5)$$

Figure 13 displays the two-dimensional contour plot for the UCS experimental data. The results support the findings which indicate ANF's are the primary contributor towards the UCS. There are fewer interactions between independent variables, indicated by the distorted parabolic contours (Nassar et al. 2016).

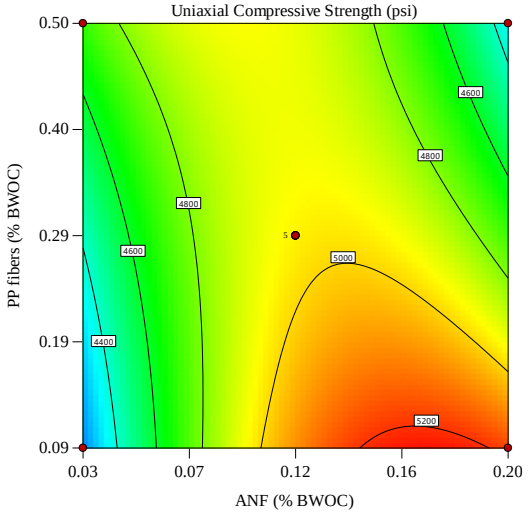

Figure 13: 2-D contour plot, UCS

RSM Analysis: Modulus of Elasticity (MOE)

Figure 14 displays the MOE values for the cement specimens which varied between 1.79 and 2.20 psi × 10^6.

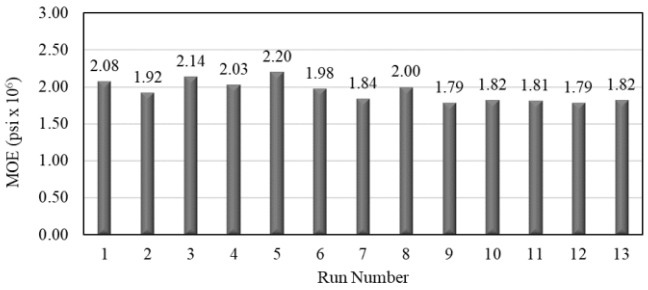

Figure 14: MOE experimental values

The values in Figure 14 were then used to develop the three-dimensional response surface plot (Figure 15).

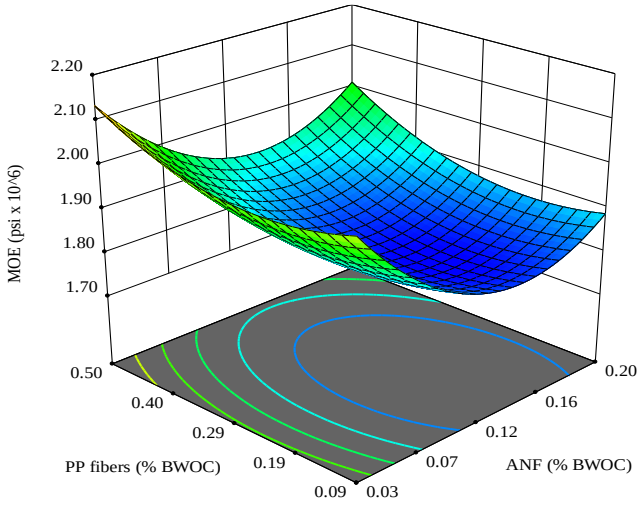

Figure 15: 3-D response surface plot, MOE

According to Figure 15, both PP fibers and ANF contribute towards obtaining the minimum MOE. Lowering the MOE of the cement sheath is advantageous because this allows the cement sheath to become more resistant to various mechanical stresses (Kopp et al. 2000). Both PP fibers and ANF are considered flexible materials in oil well cement specimens (Song et al. 2005; McElroy et al. 2020). As seen with the tensile strength of the fibers (Table 1) there is also a two orders of magnitude difference between the MOE. However, the discrepancy between the MOE of the fibers does not render the PP fibers ineffective. Since the measurement of the dynamic MOE of the cement specimen is a nondestructive test, the ultimate strength is not reached. There is only a low inelastic deformation due to the closing of microcracks from the confining pressure. Thus, the cement sample is still within the elastic region. This means the MOE is enhanced on both the nano and microscale levels. The derived RSM equation for the MOE is displayed in Equation (6).

$$MOE\ (psi\ \times\ 10^6) = 2.27187 - 5.88508 * ANF - 0.772722 * PP\ fibers + 0.717360 * ANF * PP\ fibers + 20.95156 * ANF^2 + 1.57942 * PP\ fibers^2 \quad (6)$$

Figure 16 displays the two-dimensional contour plot for the MOE experimental data. The results support the findings which indicate PP fibers and ANF's contribute synergistically towards achieving the ultimate MOE. There is a high interaction between the two fibers, indicated by the elliptical contours.

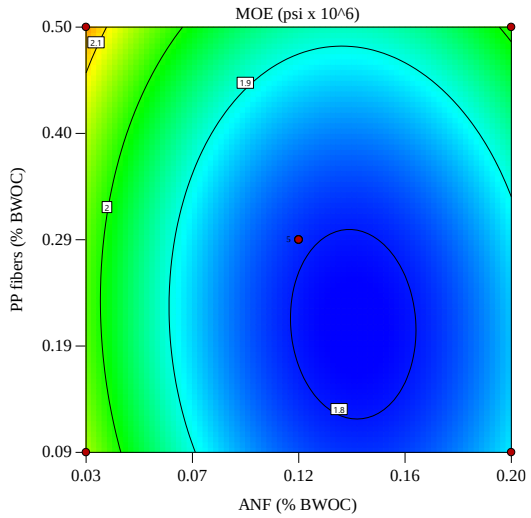

Figure 16: 2-D contour plot, MOE

Model validation using ANOVA (Analysis of Variance)

Both the UCS and MOE were effectively modeled using quadratic equations. In order to understand the relationship between the independent and dependent variables the ANOVA was utilized. Only the UCS data was used to avoid redundancy. The ANOVA results are displayed in Table 3.

Table 3: Model analysis using ANOVA

Source	Sum of Squares	df	Mean Square	F-value	p-value	Significance
Model	1.75E+06	5	3.50E+05	121.90	<0.0001	Yes
A-ANF	1.76E+05	1	1.76E+05	61.15	0.0001	Yes
B-PP fibers	5.65E+04	1	5.65E+04	19.65	0.0030	Yes
AB	4.50E+05	1	4.50E+05	156.61	<0.0001	Yes
A^2	1.05E+06	1	1.05E+06	364.11	<0.0001	Yes
B^2	1.21E+04	1	1.21E+04	4.21	0.0792	No
Residual	2.01E+04	7	2.87E+03			
Lack of Fit	1.63E+04	3	5.44E+03	5.70	0.0629	No
Pure Error	3.81E+03	4	9.53E+02			
Cor Total	1.77E+06	12				

Significant model terms are indicated by p-values less than or equal to 0.05 while insignificant model terms have p-values greater than 0.05. This means all model terms, besides the B^2 term, have a significant effect on the response. Also, the p-value of the model term indicates the quadratic model is significant. Lastly, the lack of fit p-value indicates insignificance. This means the model can be used to accurately make predictions. The summary of the regression model is presented in Table 4.

Table 4: Regression model summary

Std. Dev.	53.62		R^2	0.989
Mean	4750.15		Adjusted R^2	0.981
C.V. %	1.13		Predicted R^2	0.930
			Adeq Precision	31.460

The coefficient of variance (C.V. %) has a value less than 10% which indicates the model can be reproduced. Also, the difference between the adjusted R^2 value and the predicted R^2

value is less than 0.2; this is an indication of non-biasness. Lastly, the Adeq Precision value is greater than four which is desirable (Montgomery 2017). Figure 17 presents the normal plot of the residuals.

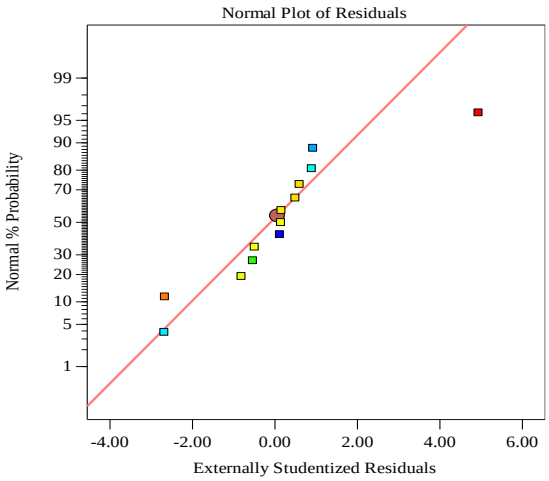

Figure 17: Normal plot of residuals

The data points fall along the inclined straight line; this indicates the data is normally distributed, which is an assumption in multiple regression. Figure 18 presents the model predicted values vs. the experimental values.

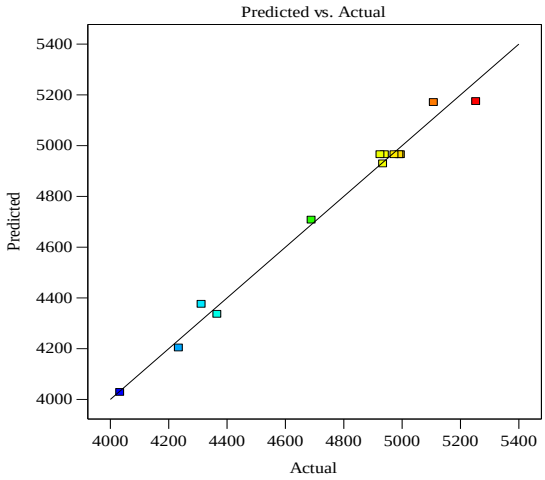

Figure 18: Predicted model values vs. experimental values

The experimental data points fall closely on the predicted model slope which indicates adequate precision. Figure 19 presents the perturbation plot.

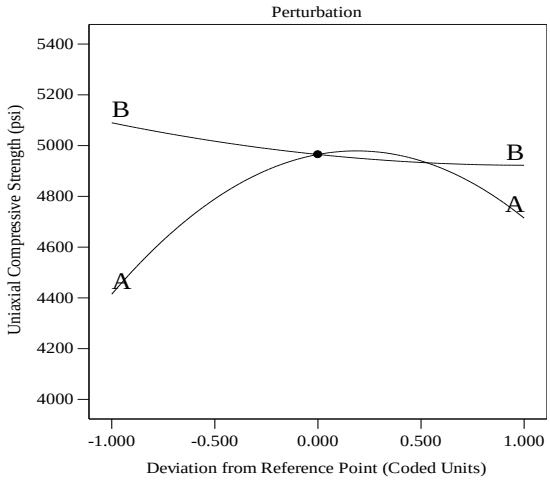

Figure 19: Perturbation plot

This plot aids in comparing the effects of ANF and PP fibers at a particular point in the design space. ANF is represented by "A" while PP fibers are represented by "B". The coded point "0" is at the centroid of the design space and the response is analyzed by changing one factor over its range while keeping the other factor constant. A flat line shows the response is insensitive to the factor, while a curved slope shows the response is sensitive to the factor. Thus, the results affirm the notation that the compressive strength is more sensitive to ANF rather than PP fibers. Similar model validating responses were also ascertained for the MOE.

Multi-variable and multi-objective optimization analysis

In order to determine the optimum concentrations of PP fibers and ANF's, a multi-variable and multi-objective optimization analysis was performed. The desirability function (DF) was used to perform the analysis (Harrington 1965; Derringer and Suich 1980). Each response (y_i) is converted into an individual desirability function (d_i), using the input variables, that vary between zero and one. Values at one signify desirability while the values at zero signify non desirability. Equation (7) is used to maximize the UCS while equation 8 is used to minimize the MOE.

$$d_i = \left(\frac{y_i - L}{U - L}\right)^{wi}, L \le y_i \le U$$

$$d_i = 0, y_i < L$$

$$d_i = 1, y_i > U \quad (7)$$

$$d_i = \left(\frac{U - y_i}{U - L}\right)^{wi}, L \le y_i \le U$$

$$d_i = 0, y_i > U$$

$$d_i = 1, y_i < L \quad (8)$$

"***L***" represents the lower limit of the response, "***U***" represents the upper limit of the response, and ***wi*** is the weight. The UCS and MOE have the same level of importance; therefore, $\boldsymbol{d_i}$ is combined using the geometric mean to calculate the overall DF (equation (9)).

$$DF = (d_1 \cdot d_2)^{1/2} \quad (9)$$

The DF for the UCS was calculated to be 0.97 and the DF for the MOE was calculated to be 0.94. The calculations resulted in a combined DF of 0.95. The optimum fiber dosages were calculated to be 0.15% ANF's (BWOC) and 0.09% PP fibers (BWOC) as shown in the ramp diagrams (Figure 20).

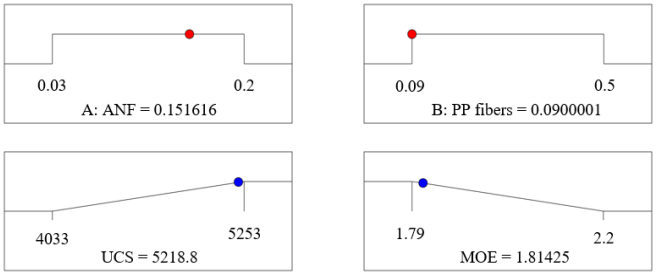

Figure 20: Ramp diagrams for optimization

Additional experimental validation tests were conducted in order to measure the accuracy of the predicted optimized values. The predicted value for the UCS (5219 psi) had a 1.33% difference from the experimentally tested sample (5150 psi). The predicted value for the MOE (1.81 psi $\times 10^6$) had a 1.10% difference from the experimentally tested sample (1.83 psi $\times 10^6$). Thus, the predicted values varied from the experimental values by less than 2%, indicating adequate precision between the measurements.

Conclusion

A fiber hybridized cement class "H" mixture, embedded with ANF's and sol-gel treated PP fibers, were experimentally investigated in this study. The UCS and MOE were investigated under simulated downhole conditions and the results were statistically analyzed. The following conclusions can be drawn:

- Based upon the results, ANF's were properly dispersed and nano-silica particles were effectively deposited on the surfaces of micro-synthetic (PP) fibers in order to enhance the fiber/matrix bond.
- After curing samples at 170 °F with 3,000 psi for 24 hours, the ultimate UCS was mainly a result of ANF reinforcement with minimum contribution from PP fibers. PP fibers provide minimum contribution due to the strength difference of the fibers and the tendency of PP fibers to resist stresses after cracks have appeared rather than before cracks appear.
- The ultimate MOE was simultaneously improved on the nano and microscale levels from the contributions of both ANF and PP fibers. The improvement is plausible because both fibers are flexible materials and the cement specimens are still within the elastic region.
- Both responses were modeled effectively using the RSM approach. Responses were modeled using quadratic formulations with model p-values less than 0.05 according to the ANOVA table. The lack of fit is not significant, and the model can be used to effectively navigate the design space according to the regression model summary.
- 0.15% ANF (BWOC) and 0.09% PP fibers (BWOC) were considered the optimum fiber concentrations based upon the multi-variable and multi-objective optimization analysis. The experimental validation tests reaffirmed the results with less than 2% variation from the predicted values.

Acknowledgments

The authors would like to thank Halliburton for providing cement class "H" and other additives. The authors would also like to thank MiniFIBERS, Inc. (USA) for providing the PP fibers. Lastly, the authors would like to acknowledge the Experimental Science Building at Texas Tech University for assisting in conducting the SEM and TEM analysis.

References

1. Aghayan, M. (2016). Functionalization of Alumina nanofibers with metal oxides, PhD thesis, Tallinn University of Technology.
2. Ahmed, A., Elkatatny, S., Gajbhiye, R., Rahman, M. K., Sarmah, P., & Yadav, P. (2018). Effect of Polypropylene Fibers on Oil-Well Cement Properties at HPHT Condition. Paper presented at the SPE Kingdom of Saudi Arabia Annual Technical Symposium and Exhibition.
3. Ahmed, A., Gajbhiye, R., Elkatatny, S., Kalimur Rahman, M., Sarmah, P., & Yadav, P. (2018). Enhancing the Cement Quality Using Polypropylene Fibers. Paper presented at the SPE Trinidad and Tobago Section Energy Resources Conference.
4. Akhlaghi, M. A., Bagherpour, R., & Kalhori, H. (2020). Application of bacterial nanocellulose fibers as reinforcement in cement composites. Construction and Building Materials, 241, 118061.
5. API, R. (2013). 10B-2: Recommended Practice for Testing Well Cements. API Recommended Practice B, 10.
6. Banthia, N., & Sappakittipakorn, M. (2007). Toughness enhancement in steel fiber reinforced concrete through fiber hybridization. Cement and Concrete Research, 37(9), 1366-1372.
7. Bly, M. (2011). Deepwater Horizon accident investigation report: Diane Publishing.
8. Coppola, B., Di Maio, L., Scarfato, P., & Incarnato, L. (2015). Use of polypropylene fibers coated with nano-silica particles into a cementitious mortar. Paper presented at the AIP Conference Proceedings.
9. Davies, R. J., Almond, S., Ward, R. S., Jackson, R. B., Adams, C., Worrall, F., Herringshaw, L. G., Gluyas, J. G., Whitehead, M. A. (2014). Oil and Gas Wells and Their Integrity: Implications for Shale and Unconventional Resource Exploitation. Marine and Petroleum Geology, 59, 674–675. doi:10.1016/j.marpetgeo. 2014.07.014.
10. Derringer, G., & Suich, R. (1980). Simultaneous optimization of several response variables. Journal of quality technology, 12(4), 214-219.
11. Di Maida, P., Radi, E., Sciancalepore, C., & Bondioli, F. (2015). Pullout behavior of polypropylene macro-synthetic fibers treated with nano-silica. Construction and Building Materials, 82, 39-44.
12. Ede, A. N., & Ige, A. (2014). Optimal polypropylene fiber

content for improved compressive and flexural strength of concrete. IOSR Journal of Mechanical and Civil Engineering (IOSR-JMCE), 11(3), 129-135.
13. El-Gamal, S., Hashem, F., & Amin, M. (2017). Influence of carbon nanotubes, nanosilica and nanometakaolin on some morphological-mechanical properties of oil well cement pastes subjected to elevated water curing temperature and regular room air curing temperature. Construction and Building Materials, 146, 531-546.
14. Hari, R., & Mini, K. (2019). Mechanical and durability properties of sisal-Nylon 6 hybrid fibre reinforced high strength SCC. Construction and Building Materials, 204, 479-491.
15. Harrington, E. C. (1965). The desirability function. Industrial quality control, 21(10), 494-498.
16. Kopp, K., Reed, S., Foreman, J., Carty, B., & Griffith, J. (2000). Foamed cement vs. conventional cement for zonal isolation-case histories. Paper presented at the SPE Annual Technical Conference and Exhibition.
17. Jafariesfad, N., Geiker, M. R., Gong, Y., Skalle, P., Zhang, Z., & He, J. (2017). Cement sheath modification using nanomaterials for long-term zonal isolation of oil wells. Journal of Petroleum Science and Engineering, 156, 662-672.
18. Khitab, A., & Tausif Arshad, M. (2014). Nano construction materials. Reviews on advanced materials science, 38(2).
19. Lavrov, A., & Torsæter, M. (2016). Physics and mechanics of primary well cementing: Springer.
20. Li, B., Li, H., Zhou, F., Guo, B., & Chang, X. (2017). Effect of cement sheath induced stress on well integrity assessment in carbon sequestration fields. Journal of Natural Gas Science and Engineering, 46, 132-142.
21. McElroy, P., Emadi, H., Surowiec, K., & Casadonte, D. J. (2019). Mechanical, rheological, and stability performance of simulated in-situ cured oil well cement slurries reinforced with alumina nanofibers. Journal of Petroleum Science and Engineering, 183, 106415.
22. McElroy, P. D., Emadi, H., & Unruh, D. (2020). Permeability and elastic properties assessment of alumina nanofiber (ANF) cementitious composites under simulated wellbore cyclic pressure. Construction and Building Materials, 239, 117867.
23. Meller, N., Kyritsis, K., & Hall, C. (2009). The mineralogy of the CaO–Al2O3–SiO2–H2O (CASH) hydroceramic system from 200 to 350 C. Cement and Concrete Research, 39(1), 45-53.
24. Metaxa, Z. S., Konsta-Gdoutos, M. S., & Shah, S. P. (2010). Mechanical properties and nanostructure of cement-based materials reinforced with carbon nanofibers and polyvinyl alcohol (PVA) microfibers. Special Publication, 270, 115-124.
25. Montgomery, D. C. (2017). Design and analysis of experiments: John wiley & sons.
26. Mueller, D. T., GoBoncan, V., Dillenbeck, R. L., & Heinold, T. (2004). Characterizing casing-cement-formation interactions under stress conditions: impact on long-term zonal isolation. Paper presented at the SPE Annual Technical Conference and Exhibition.
27. Muzenski, S., Flores-Vivian, I., & Sobolev, K. (2019). Ultra-high strength cement-based composites designed with aluminum oxide nano-fibers. Construction and Building Materials, 220, 177-186.
28. Nassar, A. I., Thom, N., & Parry, T. (2016). Optimizing the mix design of cold bitumen emulsion mixtures using response surface methodology. Construction and Building Materials, 104, 216-229.
29. Nelson, D. E. B., & Guillot, D. (2006). Well cementing second edition. Sugar land, Texas: Schlumberger.
30. Pająk, M. (2016). Investigation on flexural properties of hybrid fibre reinforced self-compacting concrete. Procedia Engineering, 161, 121-126.
31. Pinto, R. J., Marques, P. A., Barros-Timmons, A. M., Trindade, T., & Neto, C. P. (2008). Novel SiO2/cellulose nanocomposites obtained by in situ synthesis and via polyelectrolytes assembly. Composites Science and Technology, 68(3-4), 1088-1093.
32. Ramos, X., Martinez, C., Hunter, W., & Ravi, K. (2009). Three Levels of Zonal-Isolation Assurance Deployed To Maximize Life of Well Cement-Sheath Reliability and Value: Case Histories From Latin America. paper SPE, 121310.
33. Song, P., Hwang, S., & Sheu, B. (2005). Strength properties of nylon-and polypropylene-fiber-reinforced concretes. Cement and Concrete Research, 35(8), 1546-1550.
34. Yao, W., Li, J., & Wu, K. (2003). Mechanical properties of hybrid fiber-reinforced concrete at low fiber volume fraction. Cement and Concrete Research, 33(1), 27-30.